Improved Photocatalytic Activity of ZnO Film Prepared via Green Synthesis Method Using Red Watermelon Rind Extract

Ari Sulistyo Rini
Department of Physics, Mathematics and Natural Sciences, Universitas Riau

Rati, Yolanda
Department of Physics, Mathematics and Natural Sciences, Institut Teknologi Bandung

Fadillah, Raysa
Department of Physics, Mathematics and Natural Sciences, Universitas Riau

Farma, Rakhmawati
Department of Physics, Mathematics and Natural Sciences, Universitas Riau

他

https://doi.org/10.5109/6625718

出版情報：Evergreen. 9 (4), pp.1046-1055, 2022-12. 九州大学グリーンテクノロジー研究教育センター
バージョン：

Improved Photocatalytic Activity of ZnO Film Prepared via Green Synthesis Method Using Red Watermelon Rind Extract

Ari Sulistyo Rini[1,*], Yolanda Rati[2], Raysa Fadillah[1], Rakhmawati Farma[1], Lazuardi Umar[1], Yan Soerbakti[1]

[1]Department of Physics, Mathematics and Natural Sciences,Universitas Riau, Indonesia

[2]Department of Physics, Mathematics and Natural Sciences, Institut Teknologi Bandung, Indonesia

*Author to whom correspondence should be addressed:
E-mail: ari.sulistyo@lecturer.unri.ac.id

(Received August 11, 2022; Revised October 21, 2022; accepted November 30, 2022).

Abstract: In this study, the zinc oxide (ZnO) films have been prepared via the green-synthesis method with rind extract of red watermelon (*Citrullus lanatus*) as bio-stabilizer, at various acidity (pH) conditions. The ZnO films were prepared as thin films by spin-coating colloidal ZnO onto a glass substrate. The physical properties of ZnO films were characterized using UV-Vis spectrophotometer, XRD, SEM/EDX, and FTIR. The photocatalytic activity of ZnO films was evaluated systematically in the degradation process of methylene blue (MB). The sample prepared at pH 12 possesses the highest purities and exhibits the maximum degradation percentage of 94.61%, with a reaction rate constant of 0.019 min^{-1}. The efficiency of the ZnO photocatalyst has a strong correlation with the pH value in the synthesis process. Based on the results of this study, ZnO films prepared via green synthesis using *Citrullus lanatus* show an effective photocatalytic activity in degradation of MB, so that it could be developed in the photocatalytic process of water purification.

Keywords: *Citrullus lanatus*; green synthesis; photocatalytic; red watermelon rind; ZnO

1. Introduction

Organic dyes originating from modern industries such as textiles, paper, food, and rubber are harmful to the environment. Conventional techniques for removing organic dyes, such as coagulation, coprecipitation, biodegradation, filtration, and adsorption, give a relatively low level of purification and potentially provide toxic by-products[1)]. Thus, it needs to involve another purification technology to achieve desired water quality. The photocatalytic oxidation process is the most realistic solution in water purification processes[2,3)], due to its high efficiency, low cost, and environmentally friendly[4)]. Because it could effectively remove different kinds of organic dyes, research on photocatalytic materials is gaining popularity[5)].

In the photocatalytic process, the degradation of organic dyes involves a semiconductor material to produce highly reactive oxidizing species for the oxidation of pollutants[6)]. Zinc oxide (ZnO), CeO_2, ZrO_2, TiO_2, and other oxides are frequently used as photocatalysts to breakdown organic pollutants into simpler soluble compounds[1,7)]. Among these semiconductors, ZnO is very well applied as a photocatalyst due to its high electron mobility, wide bandgap energy (3.37eV), and high exciton binding energy (60 meV)[8)]. ZnO material is also environmentally friendly, easy to obtain, non-toxic, and safer than other metal nanoparticles[9)].

Photocatalyst activity is determined by the ability to photo-generate hole-electron pairs of a metal oxide semiconductor[10,11)]. ZnO with dimensions less than 100 nm possesses excellent surface reactivity and photocatalytic effectiveness because it can absorb more solar spectrum and light quantum[12,13)]. The surface reactivity and performance of ZnO are dependent on their shape and size, which may be influenced by the synthesis method and preparation conditions.

Photocatalyst materials are generally made in powder form to maximize contact with organic dyes[14,15)]. A powdered catalyst, on the other hand, needs a water separation process after the photocatalyst is completed[16)]. An application of ZnO thin film to reduce several pollutants has gained much attention. Physical techniques to fabricate ZnO thin film such as chemical vapor deposition[17)], magnetron sputterin[18)], and laser evaporation[2], offered high accuracy, but they require high costs to provide the equipments[19)]. However, another highly advantageous physical technique is spin-coating which offers low-cost fabrication, uniform growth, smooth surfaces, and simple working principles

[20,21]. In addition, ZnO thin film prepared via the wet chemical method may improve photocatalytic activity[22]. However, wet chemical methods may result in other harmful waste to the environment.

Several studies have found that the crystalline structure of ZnO nanoparticles derived from plant extracts is related to effective dye degradation. Rupa *et al.* (2019) has created crystalline-shaped ZnO nanoflowers utilizing an active ingredient found in sea buckthorn fruit to create crystalline nanoparticles that may increase the photodegradation rate of industrial dye[23]. ZnO nanoparticles synthesized utilizing extracts from various parts of the *Heliotropium indicum* performed a remarkable photocatalytic degradation of methylene blue (MB) dyes with high photocatalytic efficiency of up to 90%[24]. ZnO photocatalyst by a green method using lemon juice shows a semispherical particle with the size of 21.5 nm. In the degradation of methyl orange, methyl red, and methylene blue dye solutions, ZnO nanoparticles shown improved photocatalytic activity[25]. A green chemistry synthesis of *Gynostemma pentaphyllum* based zinc oxide by the co-precipitation approach shown a decolorization performance of 89% removing hazardous dye malachite green under UV illumination[26]. Green synthesis ZnO nanoparticles mostly exhibits better optical and intensity emission peaks[24]. Various ZnO microstructures such as nanorod[27], spherical[28], and quasi-spherical[29] have also been produced using as *Sambucus ebulus*[30] and *Ananas comosus*[31] extracts. The hexagonal nanoparticle structure of ZnO might generate more active site to interact with the toxic dye molecules and accelerate the reaction[32].

Green synthesis-based photocatalyst films can be made using a simple and minimum equipment, with comparable performance to other methods. Green synthesis relies on bio-based reducing agents[33,34] that are foundin plants extract[35], microorganisms[36], and sea creatures[37]. Plant and biological extracts function as stabilizers, reducing agents, templates, and nucleation mediates in the growth of nanoparticles[38,39]. In this study, the discarded red watermelon (*Citrullus lanatus*) rind will be used as a bio-stabilizer by taking the extract. Red watermelon rind (RWR) was chosen because it contains phenolic compounds such as vanillic, sinapic, p-coumaric, chlorogenic, and p-hydroxybenzoic acid. The phenolic compounds act as reducing agents as well as stabilizers in ZnO nanoparticles growth[40]. The application of fruit peel extract is more desirable because it may also overcome environmental problems with a simple extraction process. Several studies related to green synthesis-based ZnO nanoparticles have been also applied in environmental remediation[41], biomedicine[42], catalysis[43], and water purification[44].

In this study, ZnO film was fabricated by spin-coating a colloidal ZnO onto a glass substrate. The colloidal ZnO mixture was obtained via the green-synthesis method using RWR extract at various acidities (pH). The physical properties of ZnO films were analyzed by UV-Vis spectroscopy, XRD, SEM/EDX and FTIR. The photocatalytic activity was evaluated in the degradation process of MB.

2. Materials and methods

The research conducted is to observe MB degradation from ZnO nanoparticles photocatalyst activity with the help of bio-stabilizer from RWR waste extract. There are several important steps that need to be done such as preparation of RWR extract, fabrication of ZnO synthesis, characterization, and photocatalyst test. Utilization of organic waste such as RWR as a bio-stabilizer is highly recommended, especially the nature of ZnO which is non-toxic and environmentally friendly, so as to reduce and prevent unwanted waste. The synthesis of nanoparticles using green extract is considered very practical because the source is easy to find, besides that the source used is unused green waste so it has a higher economic value.

2.1 Preparation of RWR extract

Citrullus lanatus was purchased from a local market in Pekanbaru, Riau Province, Indonesia. The RWR was cut into small pieces up to 1 cm in size using a sterile knife and then dried in the sun to remove the moisture content. The dried rind was ground to get a powder form. 5 grams of RWR powder was dissolved in 200 ml of deionized water and heated at 80°C for 30 minutes while stirring[45]. The extract was filtered using Whatman filter paper and stored in the refrigerator at 4°C.

2.2 Greensynthesis of ZnO films

About 50 ml of RWR extract with a concentration of 25 g/l was heated at constant temperature of 80°C for 23 minutes[46]. Then, zinc nitrate hexahydrate solution (0.335M) was added to the RWR extract. The sample pH was varied by adding sodium hydroxide solution (0.1M) to obtain a pH of 6, 8, 10, and 12. The sample was heated at 80°C while stirring using a magnetic stirrer until colloidal ZnO was formed. Subsequently, 1 ml of ZnO colloid was coated onto a glass slide substrate which had been cleaned successively with DI water, acetone, and ethanol under sonication for 15 minutes at a temperature of 30°C. ZnO colloid was dripped onto the substrate and spin-coated at 2000 rpm (AC220V/20Hz/40W) for 30 seconds followed by heating at 100°C. The coating process was carried out 20 times, so that the ZnO colloid was evenly distributed on the substrate. After that, the crystallization process was carried out by annealing the ZnO film at a temperature of 400°C for 3 hours[47].

2.3 Characterization techniques

UV-Vis absorption properties, structural properties, morphology along with elemental composition, and functional groups of ZnO films were analyzed using a

UV-VIS spectrophotometer analytic Jena type Specord 200 Plus, Shimadzu 7000 diffractometer with Cu-Kα radiation (λ = 1.54056 Å), SEM with energy dispersive X-ray (SEM-EDX) FEI Inspect-S50 type and FTIR spectroscopy Prestige 2100, respectively.

2.4 Photocatalytic activity test

The photocatalytic activity of the ZnO films was evaluated in the degradation of MB solution under ultraviolet light. The ZnO film was placed in 50 ml of 10 ppm MB solution, and the adsorption-desorption process was carried out for 1 hour. The MB solution was then irradiated using a 40 Watt ultraviolet-C lamp (λ = 253.7 nm) at 25 cm distance. During the irradiation, the MB solution was stirred using a magnetic stirrer, so that the ZnO film, which acts as a catalyst material, could work homogeneously. 3 ml of test solution was sampled every 30 minutes. The sampled solutions were then evaluated using a UV-Vis Spectrophotometer before irradiation and after irradiation every 30 minutes. The rate of degradation was determined from the absorption peak of MB at a wavelength of 664 nm using a first-order kinetic equation model:

$$\ln\left[\frac{A}{A_0}\right] = -kt \quad (1)$$

and efficiency of degradation is calculated using the following equation:

$$DE = \frac{A_0 A_t}{A_0} \times 100\% \quad (2)$$

where, DE is degradation efficiency, A_0 is the initial absorbance, A_t is the absorbance at time t (minutes), and k reaction rate constants are determined from the curve gradient of $\ln[A/A_0]$ versus time (t)[48].

3. Results and discussion

The results of the green synthesis of ZnO were analyzed from several characterization techniques such as UV-Vis spectrometer, XRD, SEM/EDX, and FTIR spectroscopy. In addition, the absorption spectrum of the ZnO photocatalyst test results was also carried out at the MB concentration. This aims to determine the nature of the green synthesis of ZnO based on RWR extract as a bio-stabilizer that has been made.

3.1 UV-Vis absorption spectrum analysis

Figure 1 shows the UV-Vis absorption spectrum of ZnO films synthesized using RWR extract. ZnO films at pH variations of 6, 8, 10, and 12 gave maximum absorbance of 1.277, 1.382, 1.431, and 1.519, respectively. Based on these results, it can be said that the greater the pH value, the better the absorption ability of ZnO[49]. It implies that the level of pH affects the growth rate of ZnO. The higher the pH, the faster the ZnO nanoparticles are formed[50]. This is related to previous research by Alahdal *et al.* (2022), where the production of ZnO nanoparticles at the same pH 12 had optimal growth and greater absorbance compared to pH 6. However, the absorbance of ZnO nanoparticles decreased slightly when approaching pH 14 due to the low single dispersion in the formation of ZnO nanoparticles. Meanwhile, in acidic medium or lower than pH 6, ZnO nanoparticles cannot be formed because they are only formed in neutral and base medium[51]. The strong absorbance of all ZnO films produced by green synthesis is in the 300 nm to 370 nm ultraviolet wavelength region. Meanwhile, in the visible light region, ZnO absorption is weak. The absorption in this area indicates that the synthesized ZnO nanoparticles have been formed[52].

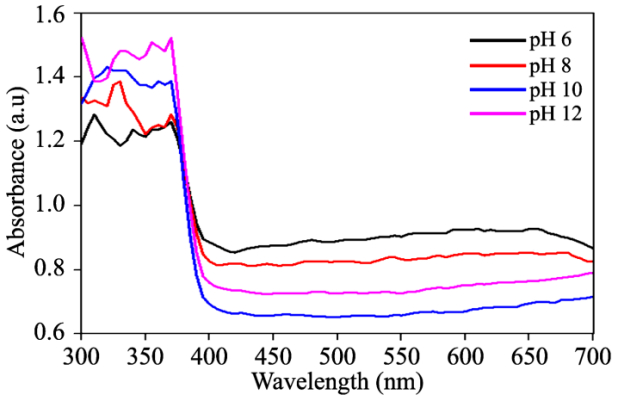

Fig. 1: UV-Vis absorbance spectrum of ZnO films.

In addition, the bandgap energy of the ZnO films was determined by the Tauc plot technique. The approach using this technique is done by extrapolating the curve $(\alpha h\upsilon)^2$ vs $(h\upsilon)$ and intercepting the x-axis, where α is the absorbance coefficient, while hυ is the energy at different wavelengths. The $(\alpha h\upsilon)^2$ vs $(h\upsilon)$ curves of ZnO films at different pH values are shown in Fig. 2.

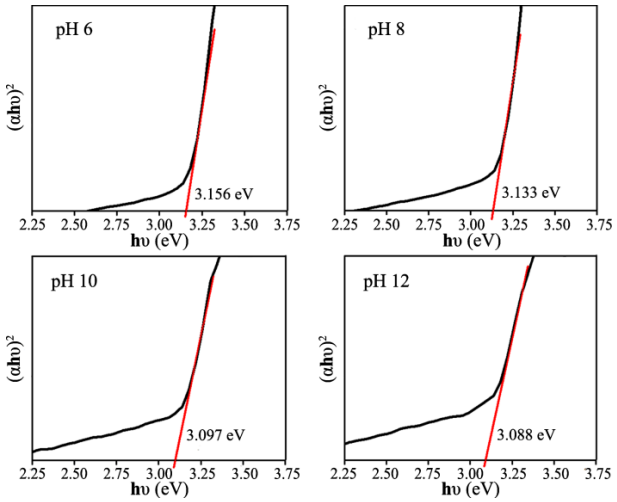

Fig. 2: The bandgap energy in the ZnO film for each pH level.

The bandgap energy of ZnO films ranges from 3.088 eV to 3.156 eV. The bandgap energy gets smaller with increasing pH value. The bandgap energy of ZnO films

obtained is lower than the ZnO's bandgap energy value, which is generally 3.37 eV[53]. These results are related to previous research by Akir *et al.* (2016) and Geetha *et al.* (2016), that has been carried out that the absorbance capacity of environmentally friendly ZnO nanoparticles based on green synthesis lies in the range of 300 nm to 400 nm with bandgap energy obtained around 3.1 eV to 4.0 eV[54,55]. The bandgap energy obtained is small enough that more electrons move to a higher energy level and absorb a lot of photons in the excited state because the distance from the valence band to the conduction band is narrow. The energy band gap has an important relationship with visible light and UV light because it is related to absorption at the wavelength of the material, so photocatalytic activity can be affected by sunlight[56]. Bandgap energy is inversely proportional to the light absorption ability of a material. The smaller the bandgap energy value, the greater the light absorption from the material[57]. Therefore, the ZnO film produced from this method has the potential to be applied as a photocatalyst.

3.2 XRD analysis

Figure 3 shows the diffraction pattern of ZnO films analyzed from XRD characterization. In the crystal plane (100), the crystalline intensity of ZnO increased with increasing pH value. In addition, an increase in the pH value indicates a narrower and sharper diffraction peak, which is known from full width half maximum (FWHM). This indicates that the higher the pH value, the higher the crystallinity[58]. The crystallinity properties were analyzed from the size of the crystals and the lattice parameters of the ZnO films, which are shown in Table 1. The crystal size of the ZnO films increases with adding pH value, where the crystal growth that occurs is getting faster. The lattice parameter obtained from each ZnO film is almost the same, with a = ~3.241 Å and c = ~5.185 Å. The size of this lattice parameter is not much different from the size of the ZnO lattice parameter in general, that the value of a is 3.249 Å and c is 5.205 Å[59].

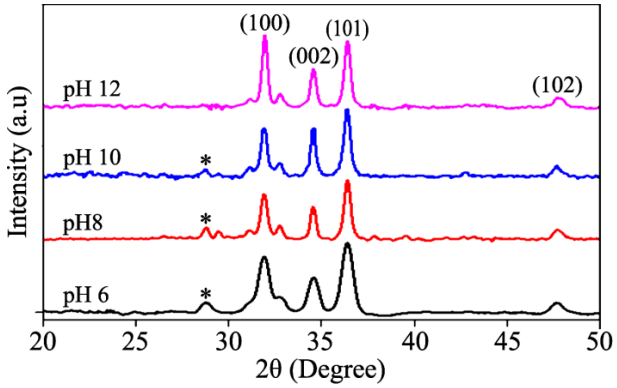

Fig. 3: XRD pattern of ZnO films.

There is an asterisk (*) in the diffraction pattern of Fig. 3 which indicates an impurity originating from the bioactive compounds in the RWR extract. These results have been previously reported[47]. In addition, there is also a diffraction peak that appears at 32° to 33° which is confirmed to contain impurities. This is also based on the reference of previous studies, where the impurity diffraction peak looks more intense and narrows on the side of the diffraction peak of the formed ZnO film crystal[60]. RWR extract has succeeded in acting as a stabilizer as well as a reducing agent in mediating the growth of ZnO nanoparticles, as in previous studies using potato extract in removing impurities from ZnO nanoparticles[61]. The ZnO phase of the sample is present at a diffraction angle of 31.89°, 34,55°, 36.37°, and 47.62° with hkl planes (100), (002), (101), and (102) (JCPDS No. 36-1451). This diffraction pattern gives a hexagonal wurtzite type ZnO crystal structure. The advantage of this wurtzite structure is that it can facilitate the excitation of electrons because the crystal structure is arranged repeatedly, so it is very well utilized in the photocatalyst process[57].

Table 1. Crystal sizes and lattice parameters of ZnO films.

Sample	2θ (°)	FWHM (Rad)	Crystal sizes (nm)	*a* (Å)	*c* (Å)
pH 6	36.32341	0.01095	13.918	3.274	5.185
pH 8	36.33342	0.00971	15.702	3.245	5.190
pH 10	36.37196	0.00892	17.103	3.241	5.190
pH 12	36.36523	0.00790	19.290	3.241	5.194

3.3 SEM-EDX analysis

Figure 4 shows the surface morphology and particle size distribution graph of ZnO films based on SEM image with a magnification of 50,000 times. The surface morphology of the obtained ZnO films is a spherical shape. This morphological form has also been reported in previous studies using Soka leaf extract (*Ixora coccinea*) as a reducing agent in ZnO formation[38]. Based on these SEM images, the difference in pH values did not affect the morphological changes of the ZnO particles. Table 2 shows the particle size for ZnO films and their standard deviations. ZnO films particle size ranged from 78.72 nm to 92.28 nm. The ZnO film sample at pH 6 had the smallest and most uniform particle size compared to other samples. The greater the pH value during the synthesis process, the greater the agglomeration that occurs, so that the particle size becomes larger[62]. Overall, the formed ZnO particles have almost uniform sizes, evidenced by their low standard deviation values or about < 20 nm.

Table 2. Particle sizes of ZnO films.

Sample ZnO	Particle Size (nm)
pH 6	78.72 ± 12.52
pH 8	85.10 ± 14.50
pH 10	90.36 ± 15.57
pH 12	92.28 ± 15.30

Information about the elemental composition of ZnO films was characterized based on the energy dispersive X-ray shown in Fig. 5. The purity of the ZnO films was proven by the elemental composition of the ZnO films. The purest sample of ZnO films only contained zinc (Zn) and oxygen (O) without were any other elements found at the pH 12 sample. Meanwhile, the samples with the most impurities, such as silicon (Si), calcium (Ca), and magnesium (Mg) were contained at pH 6. Therefore, it explains that the greater the pH value, the purer the ZnO formed. These other elements are due to the bioactive compounds found in RWR extract, which are used as reducing agents. Similar results were also obtained previously using *Albizia lebbeck* stem bark extract[50].

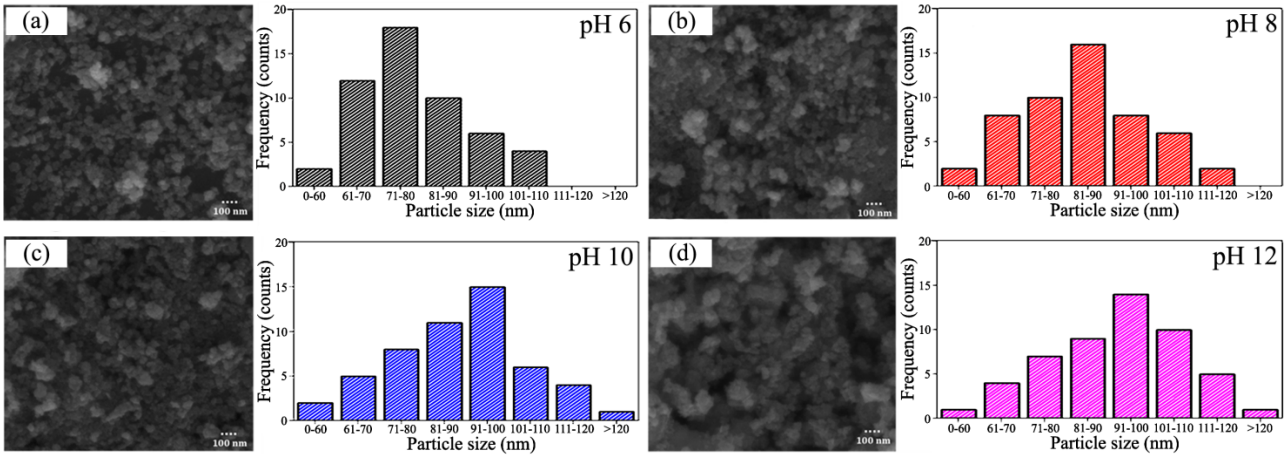

Fig. 4: SEM images and histograms of particle size distribution of ZnO films based on (a) pH 6, (b) pH 8, (c) pH 10, and (d) pH 12.

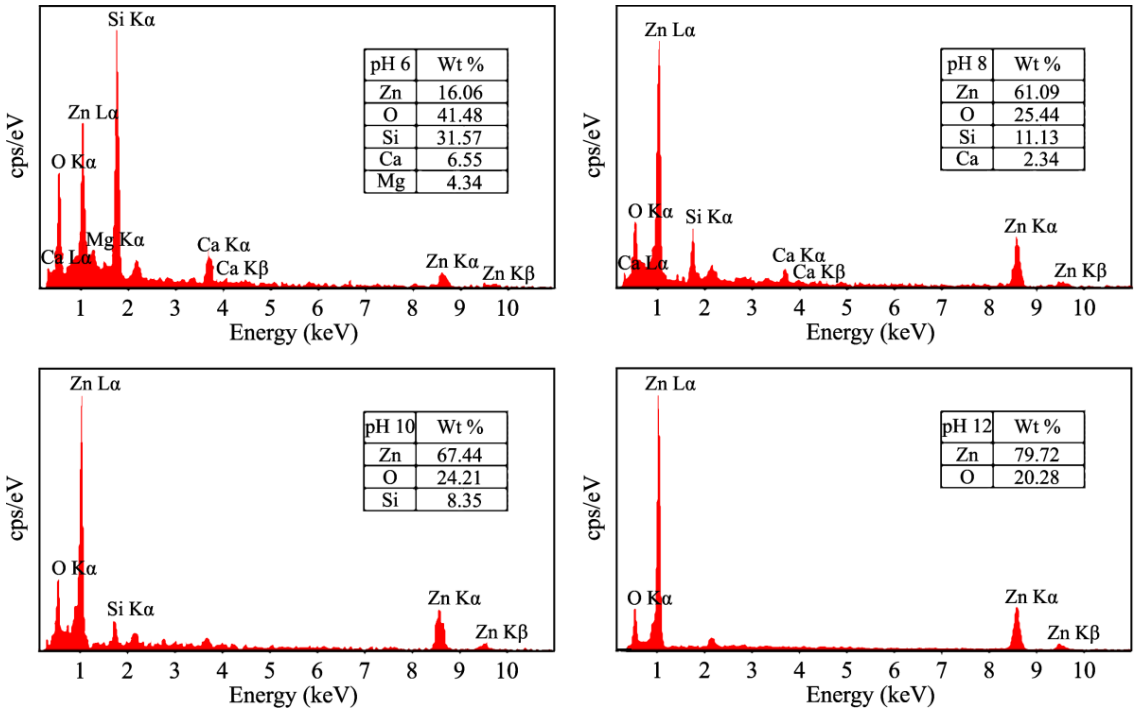

Fig. 5: EDX spectrum in determining the elemental composition of ZnO films with different pH levels.

3.4 Functional group analysis

Figure 6 shows the infrared spectrum of the compound bonding group from ZnO colloids with the green synthesis method using RWR extract. The functional groups of ZnO samples were analyzed using FTIR spectroscopy. The absorption peaks (opposite of transmittance) of ZnO samples include O-H, C-H, N-H, C-O, C-N, and Zn-O. These absorption peaks are at different wavenumbers, which are presented in Table 3.

The absorption peak due to stretching of the O-H functional group of the ZnO sample at pH 6 was indicated by the appearance of a wide peak at 3530 cm^{-1}. The content of O-H comes from the secondary metabolite compound of RWR extract. The presence of Zn and O compound bonds was indicated by two strong absorptions at wavenumbers from 340 cm^{-1} to 550 cm^{-1}. The absorption at 340 cm^{-1} was from the E_2 mode, i.e., hexagonal ZnO. At the same time, a peak at 550 cm^{-1} is associated with deficiency and vacancy of oxygen in the ZnO complex defect. Regarding the absorption of this

Zn-O functional group, the ZnO sample pH 6 has the lowest absorption at 367 cm^{-1}. This Zn-O binding proves that the ZnO formed is in a hexagonal phase without oxygen deficiency[63].

The other absorption peaks of functional groups found in the ZnO films are alkane (C-H), amine (N-H), carboxylic acids (C-O), and aromatic compounds (C-N). Those functional groups are derived from the secondary metabolites of RWR extract. Based on Table 3, the higher pH value in the synthesis process, some compounds are vanished due to the reduction of Zn^{2+} ions to Zn^0. At pH 6, there is an absorption peak at 3149.90 cm^{-1} from stretching the O-H functional group, while at pH 8, 10, and 12, there is no absorption peak at the same position. In addition, at pH 12, there is an absorption peak at 889.24 cm^{-1} which comes from stretching of the N-H functional group. Therefore, this explains that several functional groups in RWR extract play an important role in reducing the formation of ZnO nanoparticles. Similar results have been previously reported using watermelon fruit extract[64].

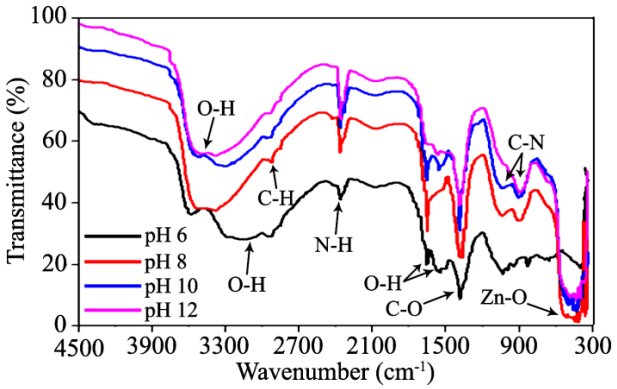

Fig. 6: FTIR spectra of ZnO samples.

Table 3. Functional groups of ZnO samples.

Functional Group	Wavenumber (cm^{-1})			
	pH 6	pH 8	pH 10	pH 12
O-H (Alcohol)	3590.39	3549.39	3532.24	3524.61
	3149.90	-	-	-
	1662.50	1653.92	1662.50	-
	1562.38	1537.59	1553.80	1570.96
C-H (Polyphenol)	2942.04	2925.83	2925.83	2924.91
N-H (Amina)	2369.01	2360.43	2369.01	2369.01
C-O (carboxylic acid)	1387.90	1379.32	1387.90	1387.90
C-N (Aromatic)	1038.93	1047.51	1030.35	-
	831.08	897.82	905.45	889.24
Zn-O (ZnO phase)	515.48 – 365.78	573.90 – 347.21	556.48 – 343.68	565.06 – 345.63

3.5 Capability of photocatalytic activity

The results of examining the photocatalytic activity of ZnO films through the degradation process of MB solution are shown in Fig. 7.

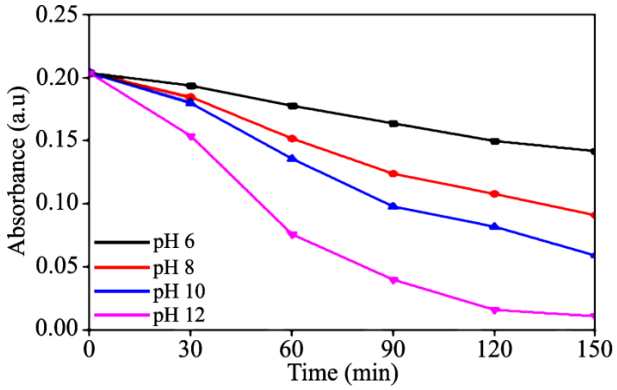

Fig. 7: Absorbance of MB solution at λ = 660 nm.

Figure 7 is the curve of MB solution absorbance at λ = 660 nm during the degradation process using ZnO films. As ZnO pH 12 sample was applied as a catalyst, the MB solution absorbance decreased drastically in 150 minutes. The photocatalytic reaction begins when the light is irradiated onto the semiconductor. The ZnO semiconductor absorbs energy and experiences electron excitation to the conduction band, leaving holes in the valence band. The holes and electrons then react with H_2O and O_2 to produce hydroxyl radicals (OH^-) and superoxide anion radicals (O_2^-) to decompose MB solution. The gap between the valence band and conduction band in this incident plays an important role in the degradation of the dye solution[65]. The narrower bandgaps cause a lot of light absorption, so that it can degrade the dye faster. This has been confirmed from the narrow bandgap energy value and the increasing pH value during the synthesis process. The ZnO sample at the highest pH has the smallest bandgap energy, which is 3.088 eV, causing this sample to degrade MB faster than other ZnO samples.

The kinetics of the reaction rate of the MB degradation process using ZnO films analyzed by plotting the $\ln[A/A_0]$ curve as a function of irradiation time is presented in Fig. 8. These results indicate that the photocatalyst activity of the ZnO films obtained follows the pseudo-first-order reaction rate law[66]. The reaction rate constant (k) is known by Eq. 2. The highest value for the reaction rate constant belongs to the pH 12

sample at the value of 0.01935 min^{-1}. These results indicate that ZnO films are suitable for efficient photocatalyst materials because they show a relatively large line slope to provide a high percentage of degradation (Fig. 9). A high percentage of degradation indicates a lot of radical formation S to decompose the MB dye[64]. The variation of the pH level of the ZnO films affects the degradation efficiency. Based on Fig. 9, the ZnO layer has the highest efficiency, with a pH 12 of 94.61%. The lowest efficiency is found at pH 6, with a degradation percentage value of 30.39%. Photocatalyst activity is also influenced by other factors such as the structure and shape of the surface. Therefore, ZnO films as photocatalysts can be potentially developed in the water purification process.

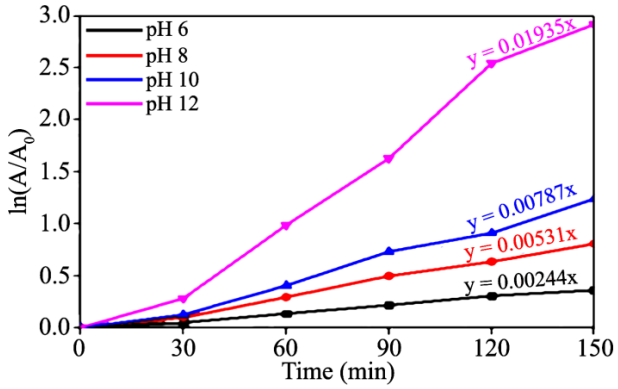

Fig. 8: Fitting plots of first-order kinetic model reaction rate.

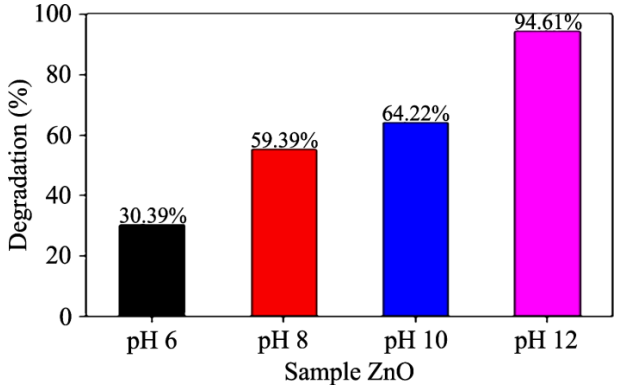

Fig. 9: Photocatalytic degradation of MB solution in ZnO films with different pH values from green synthesis.

4.Conclusion

ZnO films have been fabricated by spin-coating the green synthesized ZnO using RWR extract and applied as photocatalysts through the degradation process of MB. The optical absorption of ZnO films increases with the pH value with corresponding bandgap energy of 3.088 eV to 3.156 eV. The XRD pattern indicates that the ZnO films have a hexagonal wurtzite structure. The surface morphology of ZnO films based on SEM images is spherical. The EDX spectrum provides information that the higher the pH value of the ZnO films, the purer the sample obtained without any impurities. Based on the FTIR spectrum, there is a dominant O-H functional group on ZnO films, and the Zn-O bond is in the wavenumbers 343.68 cm^{-1} to 573.90 cm^{-1}. Photocatalyst efficiency strongly correlates with the pH conditions in the synthesis process, as supported by the analysis of its physical properties. The optimum efficient pH value of ZnO films as photocatalyst material is pH 12, with a degradation percentage of 94.61%. Based on the results of this study, ZnO films provided with the green synthesis method using RWR extract shown good photocatalytic activity and will be effective in degrading MB.

Acknowledgements

These works were supported by the Ministry of Education and Culture, the Republic of Indonesia, under Post Graduate Research Grant 2022. We thank LPPM University of Riau for facilitating this research.

References

1) G. Crini, and E. Lichtfouse, “Advantages and disadvantages of techniques used for wastewater treatment,” *Environ. Chem. Lett.*, **17** (*1*) 145–155 (2019). doi:10.1007/s10311-018-0785-9.
2) R.S. Pedanekar, S.K. Shaikh, and K.Y. Rajpure, “Thin film photocatalysis for environmental remediation: A status review,” *Curr. Appl. Phys.*, **20** (*8*) 931–952 (2020). doi:10.1016/j.cap.2020.04.006.
3) A. Azani, D.S.C. Halin, M.M.A.B. Abdullah, K.A. Razak, M.F.S.A. Razak, M.M. Ramli, M.A.A.M. Salleh, and V. Chobpattana, “The effect of GO/TiO_2 thin film during photodegradation of methylene blue dye,” *Evergreen*, **8** (*3*) 556–564 (2021). doi:10.5109/4491643.
4) M.A. Oturan, and J.J. Aaron, “Advanced oxidation processes in water/wastewater treatment: Principles and applications. A review,” *Crit. Rev. Environ. Sci. Technol.*, **44** (*23*) 2577–2641 (2014). doi:10.1080/10643389.2013.829765.
5) N.T. Nguyen, and V.A. Nguyen, “Synthesis, characterization, and photocatalytic activity of ZnO nanomaterials prepared by a green, nonchemical route,” *J. Nanomater.*, **2020** 1–8 (2020). doi:10.1155/2020/1768371.
6) A. Fauzi, L.H. Lalasari, N. Sofyan, A. Ferdiansyah, D. Dhaneswara, and A.H. Yuwono, “Titanium dioxide nanosheets derived from Indonesian ilmenite mineral through post-hydrothermal process,” *Evergreen*, **9** (*2*) 470–475 (2022). doi:10.5109/4794174.
7) S. Prabhu, T. Viswanathan, K. Jothivenkatachalam, and K. Jeganathan, “Visible light photocatalytic activity of CeO_2-ZnO-TiO_2 composites for the degradation of rhodamine B,” *Indian J. Mater. Sci.*, **2014** 1–10 (2014). doi:10.1155/2014/536123.
8) P.N. Kumar, K. Sakthivel, V. Balasubramanian, D.

Sengottaiyan, and J. Suresh, "Microwave assisted green synthesis of ZnO nanorods for dye sensitized solar cell application," *Indian J. Chem. Technol.*, **25** (*4*) 383–389 (2018). doi:10.56042/ijct.v25i4.14674.

9) A.S. Idris, S. Ghosh, H. Jiang, and K. Hamamoto, "A multi-layer stacked all sol-gel fabrication technique for vertical coupled waveguide," *Evergreen*, **4** (*2/3*) 12–17 (2017). doi:10.5109/1929657.
10) C.B. Ong, L.Y. Ng, and A.W. Mohammad, "A review of ZnO nanoparticles as solar photocatalysts: synthesis, mechanisms and applications," *Renew. Sustain. Energy Rev.*, **81** (*1*) 536–551 (2018) doi:10.1016/j.rser.2017.08.020.
11) K. Taira, and H. Einaga, "Distribution ratio of Pt on anatase and rutile TiO_2 particles, determined by X-ray diffraction and transmission electron miscroscopy analysis of Pt/TiO_2(P25)," *Evergreen*, **5** (*4*) 13–17 (2018). doi:10.5109/2174853.
12) M.C. Uribe-López, M.C. Hidalgo-López, R. López-González, D.M. Frías-Márquez, G. Núñez-Nogueira, D. Hernández-Castillo, and M.A. Alvarez-Lemus, "Photocatalytic activity of ZnO nanoparticles and the role of the synthesis method on their physical and chemical properties," *J. Photochem. Photobiol. A: Chem.*, **404** 1–10 (2021). doi:10.1016/j.jphotochem.2020.112866.
13) E.R. Dyartanti, I.N. Widiasa, A. Purwanto, and H. Susanto, "Nanocomposite polymer electrolytes in PVDF/ZnO membranes modified with PVP for use in $LiFePO_4$ Batteries," *Evergreen*, **5** (*2*) 19–25 (2018). doi:10.5109/1936213.
14) A.R. Prasad, P.R. Ammal, and A. Joseph, "Effective Photocatalytic removal of different dye stuffs using green synthesized zinc oxide nanogranules," *Mater. Res. Bull.*, **102** 116–121 (2018). doi:10.1016/j.materresbull.2018.02.022.
15) M.A. Zulfikar, A.D. Chandra, Rusnadi, H. Setiyanto, N. Handayani, and D. Wahyuningrum, "TiO_2/ZnO nanocomposite photocatalyst: Synthesis, characterization and their applicationfor degradation of humic acid from aqueous solution," *Songklanakarin J. Sci. Technol.*, **42** (*2*) 439–446 (2020). doi:10.14456/sjst-psu.2020.57.
16) V. Vaiano, and G. Iervolino, "Facile method to immobilize ZnO particles on glass spheres for the photocatalytic treatment of tannery wastewater,"*J. Colloid Interface Sci.*, **518** 192–199 (2018). doi:10.1016/j.jcis.2018.02.033.
17) I.H. Dwirekso, M. Ibadurrohman, and Slamet, "Synthesis of TiO_2-SiO_2-CuO nanocomposite material and its activities for self-cleaning," **7** (*2*) 285–291 (2020). doi:10.5109/4055234.
18) X. Wen, Q. Zhang, and Z. Shao, "Magnetron sputtering for ZnO:Ga scintillation film production and its application research status in nuclear detection," **9** (*5*) 263 (2019). doi:10.3390/cryst9050263.
19) I.A. Salimon, A.A. Temirov, I.V. Kubasov, E.A. Skryleva, A.M. Kislyuk, A.V. Turutin, D.A. Kiselev, T.S. Ilina, R.N. Zhukov, E.S. Statnik, M.D. Malinkovich, and Y.N. Parkhomenko, "Characterization of Si-DLC films synthesized by low cost plasma-enhanced chemical vapor deposition,"*Mater. Today: Proc.*, **33** 1997–2002 (2020). doi:10.1016/j.matpr.2020.06.379.
20) N.B. Patil, A.R. Nimbalkar, and M.G. Patil, "ZnO thin film prepared by a sol-gel spin coating technique for NO_2 detection," *Mater. Sci. Eng.: B*, **227** 53–60 (2018). doi:10.1016/j.mseb.2017.10.011.
21) M.I. Khan, K.A. Bhatti, R. Qindeel, H.S. Althobaiti, and N. Alonizan, "Structural, electrical and optical properties of multilayer TiO_2 thin films deposited by sol–gel spin coating," *Results Phys.*, **7** 1437–1439 (2017). doi:10.1016/j.rinp.2017.03.023.
22) W. Vallejo, A. Cantillo, B. Salazar, C. Diaz-Uribe, W. Ramos, E. Romero, and M. Hurtado, "Comparative study of ZnO thin films doped with transition metals (Cu and Co) for methylene blue photodegradation under visible irradiation," *Catalysts*, **10** (*5*) 1–13 (2020). doi: 10.3390/catal10050528.
23) E.J. Rupa, L. Kaliraj, S. Abid, D.C. Yang, and S.K. Jung, "Synthesis of a zinc oxide nanoflower photocatalyst from sea buckthorn fruit for degradation of industrial dyes in wastewater treatment," *Nanomaterials*, **9** (*12*) 1–18 (2019). doi:10.3390/nano9121692.
24) U. Wijesinghe, G. Thiripuranathar, F. Menaa, H. Iqbal, A. Razzaq, and H. Almukhlifi, "Green synthesis, structural characterization and photocatalytic applications of ZnO nanoconjugates using Heliotropium indicum," *Catalysts*, **11** (*7*) 1–21 (2021). doi:10.3390/catal11070831.
25) F. Davar, A. Majedi, and A. Mirzaei, "Green synthesis of ZnO nanoparticles and its application in the degradation of some dyes," *J. Am. Ceram. Soc.*, **98** (*6*) 1739–1746 (2015). doi:10.1111/jace.13467.
26) J.K. Park, E.J. Rupa, M.H. Arif, J.F. Li, G. Anandapadmanaban, J.P. Kang, M. Kim, J.C. Ahn, R. Akter, D.C. Yang, and S.C. Kang, "Synthesis of zinc oxide nanoparticles from Gynostemma pentaphyllum extracts and assessment of photocatalytic properties through malachite green dye decolorization under UV illumination-A green approach," *Optik*, **239** 1–11 (2021). doi:10.1016/j.ijleo.2020.166249.
27) M.G. Demissie, F.K. Sabir, G.D. Edossa, and B.A. Gonfa, "Synthesis of zinc oxide nanoparticles using leaf extract of *Lippia adoensis* (koseret) and evaluation of its antibacterial activity," *J. Chem.*, **2020** 1–9 (2020). doi:10.1155/2020/7459042.
28) B.N. Patil, and T.C. Taranath, "*Limonia acidissima* L. leaf mediated synthesis of zinc oxide nanoparticles: A potent tool against *Mycobacterium tuberculosis*," *Int. J. Mycobacteriol.*, **5** (*2*) 197–204

(2016). doi:10.1016/j.ijmyco.2016.03.004.
29) M. Ramesh, M. Anbuvannan, and G. Viruthagiri, "Green synthesis of ZnO nanoparticles using *Solanum nigrum* leaf extract and their antibacterial activity," *Spectrochim. Acta - A: Mol. Biomol. Spectrosc.*, **136** (*B*) 864–870 (2015). doi:10.1016/j.saa.2014.09.105.
30) S. Alamdari, M.S. Ghamsari, C. Lee, W. Han, H.H. Park, M.J. Tafreshi, H. Afarideh, and M.H.M. Ara, "Preparation and characterization of zinc oxide nanoparticles using leaf extract of *Sambucus ebulus*," *Appl. Sci.*, **10** (*10*) 1–19 (2020). doi:10.3390/app10103620.
31) A.S. Rini, S.D. Rahayu, Y. Hamzah, T.M. Linda, and Y. Rati, "Effect of pH on the morphology and microstructure of ZnO synthesized using *Ananas comosus* peel extract," *J. Phys.: Conf. Ser.*, **2019** (*1*) 1–7 (2021). doi:10.1088/1742-6596/2019/1/012100.
32) A. El Golli, M. Fendrich, N. Bazzanella, C. Dridi, A. Miotello, and M. Orlandi, "Wastewater remediation with ZnO photocatalysts: Green synthesis and solar concentration as an economically and environmentally viable route to application," *J. Environ. Manage.*, **286** 1–12 2021, doi:10.1016/j.jenvman.2021.112226.
33) K. Al-Hamoud, M.R. Shaik, M. Khan, H.Z. Alkhathlan, S.F. Adil, M. Kuniyil, M., M.E. Assal, A. Al-Warthan, M.R. Siddiqui, M.N. Tahir, and S.T. Khan, "*Pulicaria undulata* extract-mediated eco-friendly preparation of TiO_2 nanoparticles for photocatalytic degradation of methylene blue and methyl orange," *ACS Omega*, **7** (*6*) 4812–4820 (2022). doi:10.1021/acsomega.1c05090.
34) Q. Ouyang, F. Kou, P.E. Tsang, J. Lian, J. Xian, J. Fang, and Z. Fang, "Green synthesis of Fe-based material using tea polyphenols and its application as a heterogeneous Fenton-like catalyst for the degradation of lincomycin," *J. Clean. Prod.*, **232** 1492–1498 (2019). doi:10.1016/j.jclepro.2019.06.043.
35) A. Lagashetty, and S.K. Ganiger, "Synthesis, characterization and antibacterial study of Ag–Au Bi-metallic nanocomposite by bioreduction using piper betle leaf extract," *Heliyon*, **5** (*12*) 1–6 (2019). doi:10.1016/j.heliyon.2019.e02794.
36) H. Koopi, and F. Buazar, "A novel one-pot biosynthesis of pure alpha aluminum oxide nanoparticles using the macroalgae Sargassum ilicifolium: a green marine approach," *Ceram. Int.*, **44** (*8*) 8940–8945 (2018). doi:10.1016/j.ceramint.2018.02.091.
37) S. Safat, F. Buazar, S. Albukhaty, and S. Matroodi, "Enhanced sunlight photocatalytic activity and biosafety of marine-driven synthesized cerium oxide nanoparticles," *Sci. Rep.*, **11** (*1*) 1–11 (2021). doi:10.1038/s41598-021-94327-w.
38) S. Yedurkar, C. Maurya, and P. Mahanwar, "Biosynthesis of zinc oxide nanoparticles using *Ixora coccinea* leaf extract—A green approach," *Open J. Synth. Theory Appl.*, **5** (*1*) 1–14 (2016). doi:10.4236/ojsta.2016.51001.
39) M.A. Serunting, O.F.T. Maryana, E. Syafitri, S. Balqis, and E. Windiastuti, "Green synthesis silver nanoparticles (AgNPs) using lamtoro pods extract (*Leucaena leucocephala*) and their potential for mercury ion detection," *Evergreen*, **8** (*1*) 63–68 (2021). doi:10.5109/4372261.
40) G. Madhumitha, G. Elango, and S.M. Roopan, "Biotechnological aspects of ZnO nanoparticles: overview on synthesis and its applications," *Appl. Microbiol. Biotechnol.*, **100** (*2*) 571–581 (2016). doi:10.1007/s00253-015-7108-x.
41) J.Singh, T. Dutta, K.H. Kim, M. Rawat, P. Samddar, and P. Kumar, "'Green'synthesis of metals and their oxide nanoparticles: applications for environmental remediation," *J. Nanobiotechnol.*, **16** (*1*) 1–24 (2018). doi:0.1186/s12951-018-0408-4.
42) M. Batool, S. Khurshid, W.M. Daoush, S.A. Siddique, and T. Nadeem, "Green synthesis and biomedical applications of ZnO nanoparticles: Role of PEGylated-ZnO nanoparticles as doxorubicin drug carrier against MDA-MB-231 (TNBC) cells line," *Crystals*, **11** (*4*) 1–19 (2021). doi:10.3390/cryst11040344.
43) N. Zikalala, K. Matshetshe, S. Parani, and O.S. Oluwafemi, "Biosynthesis protocols for colloidal metal oxide nanoparticles," *Nano-Struct. Nano-Objects*, **16** 288–299 (2018). doi:10.1016/j.nanoso.2018.07.010.
44) F. Buazar, S. Alipouryan, F. Kroushawi, and S.A. Hossieni, "Photodegradation of odorous 2-mercaptobenzoxazole through zinc oxide/hydroxyapatite nanocomposite," *Appl. Nanosci.*, **5** (*6*) 719–729 (2015). doi: 10.1007/s13204-014-0368-4.
45) P.S. Ng, J.C. Sin, S.M. Lam, and Y.L. Pang, "*Citrullus lanatus* mediated-green synthesis of Ag/ZnO composite for photocatalytic degradation of 2,4-dichlorophenoxyacetic acid," *AIP Conf. Proc.*, **2157** (*1*) 1–6 (2019). doi:10.1063/1.5126578.
46) M. Ndikau, N.M. Noah, D.M. Andala, and E. Masika, "Green synthesis and characterization of silver nanoparticles using *Citrullus lanatus* fruit rind extract," *Int. J. Anal. Chem.*, **2017** 1–9 (2017). doi:10.1155/2017/8108504.
47) R. Fadillah, Y. Rati, R. Dewi, R. Farma, and A.S. Rini, "Optical and structural studies on bio-synthesized ZnO using *Citrullus lanatus* peel extract," *J. Phys.: Conf. Ser.*, **1816** (*1*) 1–7 (2021). doi:10.1088/1742-6596/1816/1/012019.
48) S. Balu, K. Uma, G.T. Pan, T.C.K. Yang, and S.K. Ramaraj, "Degradation of methylene blue dye in the presence of visible light using SiO_2@α-Fe_2O_3 nanocomposites deposited on SnS_2 flowers," *Materials*, **11** (*6*) 1–17 (2018). doi:10.3390/ma11061030.

49) M. Gupta, R.S. Tomar, S. Kaushik, R.K. Mishra, and D. Sharma, "Effective antimicrobial activity of green ZnO nano particles of *Catharanthus roseus*," *Front. Microbiol.*, **9** 1–13 (2018). doi:10.3389/fmicb.2018.02030.

50) H. Umar, D. Kavaz, and N. Rizaner, "Biosynthesis of zinc oxide nanoparticles using *Albizia lebbeck* stem bark, and evaluation of its antimicrobial, antioxidant, and cytotoxic activities on human breast cancer cell lines," *Int. J. Nanomed.*, **14** 87–100 (2019). doi:10.2147/IJN.S186888.

51) F.A. Alahdal, M.T. Qashqoosh, Y.K. Manea, M.A. Salem, A.M. Khan, and S. Naqvi, "Eco-friendly synthesis of zinc oxide nanoparticles as nanosensor, nanocatalyst and antioxidant agent using leaf extract of *P. austroarabica*," *OpenNano*, **8** 1–14 (2022). doi:10.1016/j.onano.2022.100067.

52) T. Khalafi, F. Buazar, and K. Ghanemi, "Phycosynthesis and Enhanced photocatalytic activity of zinc oxide nanoparticles toward organosulfur pollutants," *Sci. Rep.*, **9** (*1*) 1–10 (2019). doi:10.1038/s41598-019-43368-3.

53) M.J. Haque, M.M. Bellah, M.R. Hassan, and S. Rahman, "Synthesis of ZnO nanoparticles by two different methods & comparison of their structural, antibacterial, photocatalytic and optical properties," *Nano Express*, **1** (*1*) 1–13 (2020). doi:10.1088/2632-959x/ab7a43.

54) S. Akir, A. Barras, Y. Coffinier, M. Bououdina, R. Boukherroub, and A.D. Omrani, "Eco-friendly synthesis of ZnO nanoparticles with different morphologies and their visible light photocatalytic performance for the degradation of Rhodamine B," *Ceram. Int.*, **42** (*8*) 10259–10265 (2016). doi: 10.1016/j.ceramint.2016.03.153.

55) M.S. Geetha, H. Nagabhushana, and H.N. Shivananjaiah, "Green mediated synthesis and characterization of ZnO nanoparticles using Euphorbia Jatropa latex as reducing agent," *J. Sci.: Adv. Mater. Devices*, **1** (*3*) 301–310 (2016). doi: 10.1016/j.jsamd.2016.06.015.

56) P. Chen, H. Liu, W. Cui, S.C. Lee, L.A. Wang, and F. Dong, "Bi-based photocatalysts for light-driven environmental and energy applications: structural tuning, reaction mechanisms, and challenges," *EcoMat*, **2** (3) 1–30 (2020). doi:10.1002/eom2.12047.

57) E.A. Araújo, F.X. Nobre, G.D.S. Sousa, L.S. Cavalcante, M.R.D.M.C. Santos, F.L. Souza, and J.M.E. de Matos, "Synthesis, growth mechanism, optical properties and catalytic activity of ZnO microcrystals obtained via hydrothermal processing," *RSC Adv.*, **7** (*39*) 24263–24281 (2017). doi:10.1039/c7ra03277c.

58) M.F. Kasim, N. Kamarulzaman, R. Rusdi, and A.A. Rahman, "Effect of pH on the crystal growth of ZnO nanomaterials and their band gap energies," *J. Phys.: Conf. Ser.*, **1083** (*1*) 1–5 (2018). doi:10.1088/1742-6596/1083/1/012043.

59) R. Elilarassi, and G. Chandrasekaran, "Structural, optical and electron paramagnetic resonance studies on Cu-doped ZnO nanoparticles synthesized using a novel auto-combustion method," *Front. Mater. Sci.*, **7** (*2*) 196–201 (2013). doi:10.1007/s11706-013-0198-4.

60) E. Guziewicz, E. Przezdziecka, D. Snigurenko, D. Jarosz, B.S. Witkowski, P. Dluzewski, and W. Paszkowicz, "Abundant acceptor emission from nitrogen-doped ZnO films prepared by atomic layer deposition under oxygen-rich conditions," *ACS Appl. Mater. Interfaces*, **9** (*31*) 26143–26150 (2017). doi:10.1021/acsami.7b04127.

61) F. Buazar, M. Bavi, F. Kroushawi, M. Halvani, A. Khaledi-Nasab, and S.A. Hossieni, "Potato extract as reducing agent and stabiliser in a facile green one-step synthesis of ZnO nanoparticles," *J. Exp. Nanosci.*, **11** (*3*) 175–184 (2016). doi:10.1080/17458080.2015.1039610.

62) Siswanto, N.T. Rochman, and P.R. Akwalia, "Fabrication and characterization of zinc oxide (ZnO) nanoparticle by sol-gel method," *J. Phys.: Conf. Ser.*, **853** (*1*) 1–5 (2017). doi:10.1088/1742-6596/853/1/012041.

63) J. Lv, C. Li, and J.J. BelBruno, "Characteristics of point defects on the optical properties of ZnO: revealed by Al–H Co-doping and post-annealing," *RSC Adv.*, **3** (*23*) 8652–8656 (2013). doi:10.1039/C3RA40837J.

64) L.S.R. Yadav, D. Kumar, C. Kavitha, H. Rajanaika, B.D. Prasad, H. Nagabhushana, and G. Nagaraju, "Antibacterial and photocatalytic activities of ZnO nanoparticles: Synthesized using water melon juice as fuel," *Int. J. Nanosci.*, **15** (*1-2*) 1–8 (2016). doi:10.1142/S0219581X1650006X.

65) A. Venkateasan, R. Prabakaran, and V. Sujatha, "Phytoextract-mediated synthesis of zinc oxide nanoparticles using aqueous leaves extract of *Ipomoea pes-caprae* (*L*).*R.br* revealing its biological properties and photocatalytic activity," *Nanotechnol. Environ. Eng.*, **2** (*1*) 1–15 (2017). doi:10.1007/s41204-017-0018-7.

66) G. Nagaraju, Udayabhanu, Shivaraj, S.A. Prashanth, M. Shastri, K.V. Yathish, C. Anupama, and D. Rangappa, "Electrochemical heavy metal detection, photocatalytic, photoluminescence, biodiesel production and antibacterial activities of Ag–ZnO nanomaterial," *Mater. Res. Bull.*, **94** 54–63 (2017). doi:10.1016/j.materresbull.2017.05.043